

K. O. E. Henriksson,* K. Nordlund, and J. Keinonen
Accelerator laboratory, P.O. Box 43, FI-00014 University of Helsinki, Finland
 (Dated: November 24, 2004)

Using molecular dynamics simulations and the Embedded Atom Method (EAM) potential we have investigated the sputtered atom clusters produced by 15 keV xenon impacts on silver and 20 keV xenon impacts on gold. Ejected clusters were simulated for long times, up to $0.01 - 1 \mu\text{s}$, in order to investigate the fragmentation of nascent clusters. The size distributions of nascent and final clusters were calculated and fitted to an inverse power law, resulting in exponents close to 2 and 3, depending on the range of the cluster sizes used. These values are in agreement with other simulations and experiments. The results show that clusters are subject to a dramatic breakup, which makes the size of the largest sputtered cluster go down by a factor of 2 – 4. Despite this, the exponent in the power law does not change very much from the size distribution of nascent to that of final clusters. Considering the uncertainties, the exponent of the final size distribution is 1.0 – 1.7 times the exponent of the nascent size distribution.

PACS numbers: 61.80.Jh, 36.40.Qv, 83.10.Mj

I. INTRODUCTION

Atoms and atom aggregates — usually referred to as clusters — are sputtered from the surface of a metal when it is bombarded with energetic heavy ions. Sputtering has been studied analytically and experimentally over the past four decades¹. Early studies dealt mostly with charged clusters, whereas the total amount of sputtered clusters — charged and neutral ones — has been studied only during the last ten years. Since the fraction of clusters emitted in a charged state is an *a priori* unknown quantity, nothing conclusive can be said about *e.g.* the total cluster size distribution from this part alone².

During the last decade the detection of neutral sputtered clusters has become more efficient. Nowadays, a quite large groups of atoms can be identified. This is mainly due to the technique of *single photon ionization* (SPI), which utilizes ultra violet (UV) and very ultra violet (VUV) laser light to ionize neutral clusters shortly after ejection^{2,3}. Ideally, the ionization is achieved by absorption of single photons.

Clusters containing about 500 to 10000 atoms have been detected in a recent transmission electron microscopy (TEM) study⁴. In addition, clusters containing up to 60 atoms⁵ and up to 200 atoms⁶ have been detected in SPI studies. In refs. 5 and 6 post-acceleration was used to improve the detection efficiency of large clusters, so the (large-cluster) results should be more reliable than the earlier ones.

There still seem to be some difficulties in obtaining the size distribution of neutral clusters using the SPI technique. These are mainly the cluster fragmentation induced by photons⁷, and the inherently lower detection efficiency of large clusters, if post-acceleration or other corrections are not carried out⁵.

Fits of the size distribution of clusters $Y(n)$ — where n is the number of atoms in the cluster — to an inverse power law $Y(n) = Y_1 n^{-\delta}$ — where Y_1 and δ are the fitting parameters — have consistently returned exponents

δ close to 2 or 3 in recent experiments⁴⁻⁶. The former value is in accordance with analytical models^{8,9}, which predict an inverse power law dependence with an exponent very close to 2. However, it should be noted that these theories predict only the distribution of *nascent* (or “newborn”) clusters — *i.e.* the clusters existing shortly after ejection — whereas experiments determine the distribution of *final* (or metastable) clusters, formed by the breakup of nascent clusters. Combining this with the fact that the fragmentation of nascent clusters can have quite an important effect on the size distribution, it seems inappropriate to compare experimental results for the exponent to those predicted by analytical theory, but this is nevertheless usually done. Comparisons to analytical exponents should be made using the size distribution of nascent clusters. However, it is not immediately obvious how the relevant measurements could be carried out, at the rapid time scale of cluster formation shortly after ion impact. It is much more straightforward to obtain the size distribution of nascent clusters using simulations. In order to verify the correctness of the simulated results, the clusters should be simulated for quite a long time so that also the distribution of final clusters — or a reasonable estimate of it — can be obtained. A favorable comparison between this distribution and the experimental distribution would then in optimal cases verify the validity of the simulated nascent distribution.

In order to investigate how significant the effect of fragmentation is and how strongly it affects the value of the size distribution exponent, we have carried out molecular dynamics simulations of 15 keV xenon ions incident on silver and 20 keV xenon ions incident on gold. In the following section we describe the simulations and the interatomic potentials, and give a short overview of alternative techniques to obtain the final or metastable clusters. Results for the total sputtering yield, the fraction of atoms in large clusters, the inverse power law exponents, and the temperature of nascent and final silver clusters are then presented and discussed.

A. Substrate and ion properties

Molecular dynamics simulations (MDS) were used to investigate the cascades produced by single-ion xenon irradiation of silver and gold (001) surfaces. In this section we will describe only the details of the MDS specific to this study. A more extensive description of our MDS for investigation of cascades can be found elsewhere¹⁰.

The initial energy of the impinging Xe ion was 15 keV for impacts on Ag surfaces and 20 keV for Au. The bulk specimen consisted of $44^2 \times 34$ and 44^3 unit cells for Ag, and 48^3 unit cells for Au. A grand total of 88 runs were completed for the case of Xe on Ag, and 29 runs for Xe on Au.

Since ion channeling may lead to dramatic increases in the ion range, and hence necessitate the use of very large simulation cells with subsequent huge demands for computational time, impact angles which minimize channeling were chosen. Combinations of polar (or tilt) angle θ and azimuthal (or twist) angle ϕ used for the ions were $\theta = \phi = 45^\circ$ for the Ag case and $\theta = \phi = 25^\circ$ for Au. The angles for Au were determined previously (see table I in ref. 11) using MD range calculations¹². By a similar procedure we obtained that $\theta = 45^\circ$ and $\phi = 45^\circ$ give a minimum average range for Xe ions in Ag, namely about 40 – 50 Å.

A free (001) surface was created for each substrate using non-periodic boundary conditions in all three directions x , y and z . In order to remove any unphysical cascade behavior caused by the walls and the bottom of the simulation cell — *e.g.* reflection of pressure waves generated by the cascade — the techniques of atom fixing and temperature scaling were employed. The scaling of temperature emulates the heat conduction into the surrounding bulk which takes place in experimental targets. In detail, atoms in a 5 Å thick layer at the walls were fixed and Berendsen temperature scaling¹³ was applied to atoms located $2a$ inward from the fixed region. Here, a is the lattice parameter taken at the initial average temperature of the bulk, 300 K. During the simulations pressure waves were produced in an early stage of the cascade. The waves propagated away from the cascade in all directions, but mainly toward the side walls of the bulk, where they were somewhat reflected back from the temperature-scaled region. However, the intensity of the reflected wave was quite low, and was not observed to affect the cascade. No obvious correlation between the sputtering yield and the reflected weak pressure waves was observed.

The initial x and y coordinates of the incident ion were selected according to a uniform distribution in the interval $[0, a]$. This corresponds to a random point in one of the six side planes of the face-centered cubic (FCC) conventional unit cell. The initial z coordinate was chosen so that the distance from the ion to the bulk was about equal to the cutoff radius of the potential.

Potentials based on the Embedded Atom Method (EAM) by Foiles *et al.*¹⁴ were used. Since in some studies it has been found that the EAM potential overbinds small clusters and thus discriminates against larger ones^{15,16}, we also tested another potential, namely the Molecular Dynamics/Monte Carlo Corrected Effective Medium potential (MD/MC-CEM), originally developed by DePristo *et al.*¹⁷. The MD/MC-CEM potential was chosen since it has been explicitly fitted to both bulk solid and dimer properties^{16,17}.

At small interatomic distances the EAM and MD/MC-CEM potentials were smoothly joined to the universal, repulsive Ziegler-Biersack-Littmark (ZBL) potential¹⁸ to realistically describe high-energy collisions and interaction of atoms at small separations. Electronic stopping¹⁸ was applied to all atoms having a kinetic energy larger than or equal to 5 eV.

The cutoff radius for the potentials was 5.55 Å (EAM) and 6.6 Å (MD/MC-CEM). The original potentials are constructed so that they go smoothly to zero when the cutoff radius is approached from below^{14,17}. In this study we did not modify these cutoff distances.

The MD/MC-CEM melting temperature for Au, 1635 ± 5 K, turned out to be quite high in comparison with the empirical melting temperature 1337 K (ref. 19), and that given by the EAM potential, 1110 ± 20 K. We obtained the EAM and MD/MC-CEM melting temperatures by simulating solid phase in contact with liquid phase at constant temperature, until only one of these phases remained. This was repeated for several different temperatures, and the type of the final phase was noted. The starting temperature around which the final phase changed from liquid to solid was considered to be the actual melting temperature.

It should be noted that it is not a given fact that the EAM potentials give a good description of clusters, since they have been mostly fitted to bulk properties¹⁴. Although the binding energies of small clusters (containing less than about 10 atoms) predicted by the EAM potential are not exactly the same as those obtained from experiments and *ab initio* calculations¹⁶, the EAM potential still gives a fairly accurate description of at least the melting and freezing of clusters^{20,21}, and the ground state atomic configuration of clusters¹⁶.

C. Simulation of ejected clusters

The evolution of the system was followed for times up to 50 ps for the gold cascades and up to 40 – 50 ps for the silver cascades. Some of the silver cascades were simulated for even longer times, in order to allow late clusters to be well separated from the irradiated bulk surface.

After the cascade simulation ended, the substrate and ejected clusters with a velocity component toward the surface and/or less than about 10 Å from the substrate

surface were removed from the simulation cell. The remaining sputtered material was subjected to clustering analysis. The cluster size distribution obtained from this analysis was called the *nascent size distribution*.

The extracted material was simulated for long times, up to 1000 ns for Xe on Ag and between 500 and 8000 ps for Xe on Au, slightly depending on the number of atoms in the simulation. The run which was ended at 8000 ps showed a cluster distribution stable for the last 1090 ps.

Most parameters in the cluster simulations retained their values from the cascade simulations. Most notably, the non-periodic boundary conditions were still enforced. However, all parameters concerning temperature scaling and atom fixing were removed. When these simulations ended, clustering analysis was carried out again. The obtained size distribution was called the *final size distribution*.

It is a reasonable assumption that the cluster decay does not continue for an unlimited time. On sufficiently large time scales black-body radiation will cool down the clusters, eventually to arbitrarily low temperatures (but never reaching exactly 0 K), which makes further fragmentation unlikely. We make an order-of-magnitude estimate of this time using the equation for black-body radiation:

$$-\frac{1}{4\pi R^2} \frac{dE}{dt} = \sigma T^4. \quad (1)$$

Here R is the radius of the approximately spherical clusters, $dE = nMC_v dT$ the energy loss, n the number of atoms in the cluster, M the atomic mass, C_v the specific heat capacity, and T the internal temperature. Solving this equation and calculating how long it takes for a cluster to cool down from the boiling temperature T_b (T_b is 2435 K for Ag and 3129 K for Au, ref. 19) to half of the melting temperature T_m (T_m is 1235 K for Ag and 1337 K for Au) — when one can assume that the cluster has crystallized and decay is highly unlikely — one obtains $t \sim 10 \mu\text{s}$ for both Ag and Au for a typical cluster size of $n \sim 100$. This estimate is not strongly dependent on the number of atoms n in the cluster or the initial temperature. This simple calculation is valid as an order-of-magnitude estimate. Experiments confirm that hot metallic nanoparticles can indeed cool down by hundreds of Kelvins on microsecond time scales^{22,23}.

D. Alternative techniques to obtain final (or metastable) clusters

There are two principal methods for obtaining the final distribution of clusters. One widely used method is the so-called *dissociation analysis* (DA)^{15,16,24,25}. DA uses MDS to create the nascent distribution of clusters. The internal energy of each cluster containing n atoms is compared to a list of threshold energies $E_{\text{th}}^{(n,m)}$ corresponding to decay modes m , in which a cluster con-

taining n atoms decays into a pair of clusters containing $n - m$ atoms and m atoms. This reaction can be shortly written as $(n) \rightarrow (n - m) + (m)$. Depending on the difference between internal energy and threshold energy for fragmentation, the clusters are considered unstable or (meta)stable.

The threshold energies are $E_{\text{th}}^{(n,m)} = E_a(n - m) + E_a(m) - E_a(n)$, where $E_a(n)$ is the atomization energy of the n -cluster (a cluster containing n atoms), *i.e.* the energy required to break the cluster into separate atoms. For $n < 10$ the atomization energies are calculated using MDS, by heating and cooling the clusters to get them into the configuration corresponding to their minimum potential energy. For larger values of n this process is too cumbersome, so usually the approximation

$$E_a(n) = U_s(1 - cn^{-\kappa}) \quad (2)$$

is used, where the constants c and κ are fitted to data, and U_s (the sublimation energy) is obtained directly from the interatomic potential. The functional form of eq. (2) is based on a liquid drop model^{15,16,25}.

Usually Monte Carlo simulations (MCS) are employed in conjunction with the above recipe for fragmentation. In this case breakup rates are obtained from *e.g.* the Rice-Ramsperger-Kassel (RRK) theory, which relates the internal energy and the threshold energy for fragmentation to the breakup rate¹⁵. Unfortunately this type of calculation does not in itself allow the breakup to be studied as a function of time, unless some scheme which relates the time steps in the MCS to physical time is used.

The following notes seem to be some of the most important shortcomings of the dissociation analysis: (i) There is no direct link between the time steps in the calculation or the Monte Carlo simulation and physical time; (ii) The calculation to obtain the atomization energies is tedious and cumbersome for large clusters (say, $n > 10$); (iii) It is not obvious to what extent the atomization energy expression in eq. (2) is a good approximation.

The simulation studies of cluster fragmentation referenced in this work (refs. 15,16,24,25) have all been done using dissociation analysis.

The second way to obtain the final distribution of clusters is to carry out full MDS of the clusters until they become stable for long times, or until the time reaches microscopic scales, say several μs . Using MDS the shortcomings of the dissociation analysis can be circumvented, making the calculations straightforward.

III. RESULTS

A. Total yield

The total sputtering yields calculated from the simulation data are displayed in table I. The data tagged with the label 'EAM' are from the calculations using the EAM

potentials, whereas 'MD/MC-CEM' refers to calculations with the corrected effective medium potential. The total yield is defined as the total number of sputtered atoms divided by the number of impinging ions.

In the table, except for the cases tagged with the label 'all', we have considered only those clusters that move away from the irradiated surface. In these calculations all clusters were considered, independent of their direction of motion.

TABLE I: Total sputtering yields. ⁽¹⁾ refers to the EAM potential, and ⁽²⁾ to the MD/MC-CEM potential. The label 'all' means that all clusters have been considered, ignoring their direction of motion (away from or toward the surface). The error is the standard deviation.

	Ag 15 keV Xe	Au 20 keV Xe
nascent ⁽¹⁾ (all)	143 ± 17	82 ± 15
nascent ⁽¹⁾	142 ± 16	79 ± 14
final ⁽¹⁾	129 ± 14	78 ± 13
nascent ⁽²⁾ (all)	-	32 ± 7

If we assume that the clusters moving toward the surface at the time of the final distribution do not fragment such that they produce clusters moving in the reverse direction (toward the detector), then the amount of re-deposited material can be estimated from the nascent yield containing all clusters, and the final yield. Using the numbers in the table, we find that the amount of re-deposited material is $1 - (129 \pm 14)/(143 \pm 17) = 10 \pm 15\%$ for 15 keV Xe on Ag and $5 \pm 24\%$ for 20 keV Xe on Au. Considering the large uncertainties, we can with confidence only state that the amount of redeposited atoms is in the range 0 – 30%.

B. Fraction of atoms in large clusters

The total sputter yield Y as well as the fraction f of atoms in large clusters (containing $n \geq 4$ atoms) are plotted in figure 1 as a function of time (up to 50 ps) for the case of 20 keV xenon bombardment of gold. Here the yield Y is defined as the total number of sputtered atoms N_{sput} divided by the number of impinging ions N_{ions} , $Y = N_{\text{sput}}/N_{\text{ions}}$. The fraction f is defined as $f = N_4/N_{\text{sput}}$, where N_4 is the number of atoms bound in clusters with sizes $n \geq 4$. Note that in figure 1 the average is shown for 20 simulations of a total of 29. In the other runs the atomistic output was taken at different times, making them unsuitable for this figure. The included runs contain relatively many large clusters, which usually means a larger amount of sputtered atoms per run. Due to this fact, the average yield in figure 1(a) is larger than that obtained when all runs are included. From the figure, the yield at 50 ps is 113 ± 25 for 20 runs, which is consistent with the value 82 ± 15 in table I for 29 runs, when considering the 1σ uncertainty.

As can be seen in figure 1(a), the number of sputtered atoms seems to have attained its maximum value at about 20 ps after ion impact. In part (b) of the figure, we see that the fraction of atoms bound in large clusters increases dramatically up to 10 ps, and essentially remains the same after that.

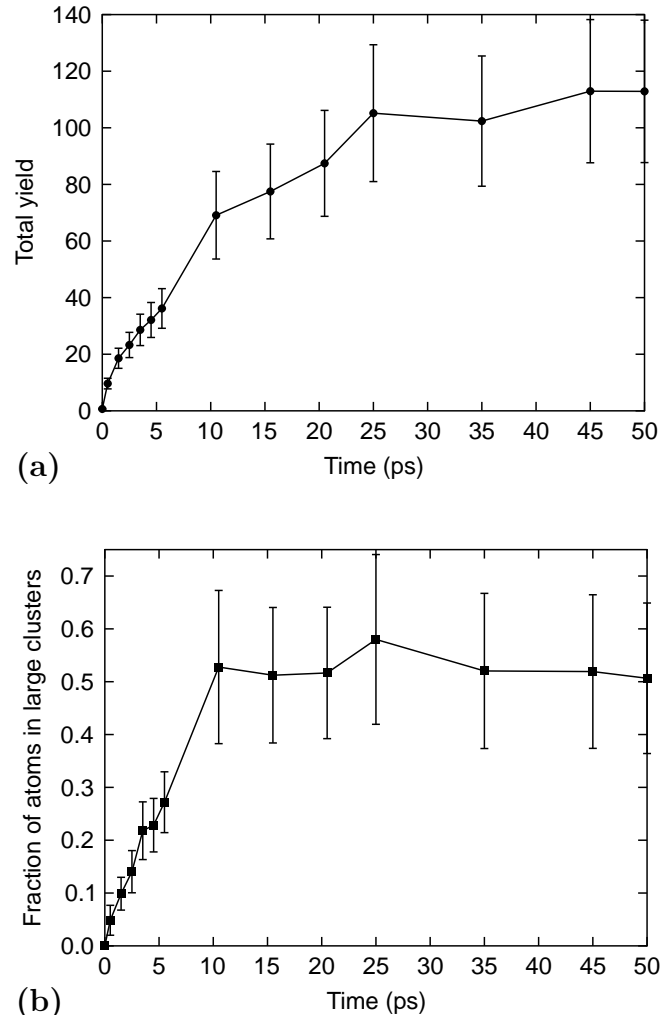


FIG. 1: Total yield (a), as well as the fraction of atoms in large clusters ($n \geq 4$) (b), as a function of time (up to 50 ps), averaged over 20 simulations of a total of 29, for 20 keV Xe on Au. The line is intended as a guide for the eye. The error is the standard deviation.

By visual inspection we observed that there is some breakup of large clusters already during the cascade regime (up to about 50 ps after ion impact), see figure 2. The reason why this is not apparent in figure 1(b) is that fragmentation is accompanied by late emission of clusters, which supply new clusters for those breaking up or falling back down onto the surface. The breakup of clusters during the cascade became clear only when the fraction of atoms in clusters with more than 100 atoms

was plotted.

In order to clarify the massive breakup of large clusters that takes place after the nascent distribution has been obtained, up to the time of the final distribution, the fraction of atoms bound in large clusters moving away from the irradiated surface has been calculated. The results are displayed in table II. Column 1 in the table shows the cluster size, whereas columns 2 and 4 show results for the nascent distribution, and columns 3 and 5 for the final distribution. For example, take the line with $N = 20$. For 15 keV Xe on Ag, column 2 indicates that at the end of the cascade simulation (the time of the nascent size distribution) $30 \pm 5\%$ of all atoms are bound in clusters that contain 20 or more atoms. Column 3 reveals that at 1000 ns (the time of the final size distribution for 15 keV Xe on Ag) only $1.5 \pm 0.7\%$ of all atoms are bound in clusters containing 20 or more atoms.

TABLE II: Fraction of atoms in clusters with sizes larger than N . Data from all simulations have been used. Only clusters moving away from the surface have been included. The error is the standard deviation.

N	15 keV Xe on Ag		20 keV Xe on Au	
	nascent (%)	final (%)	nascent (%)	final (%)
4	53 ± 5	5.0 ± 0.8	40 ± 11	21 ± 6
10	37 ± 5	2.5 ± 0.8	36 ± 11	18 ± 6
20	30 ± 5	1.5 ± 0.7	32 ± 11	14 ± 6
30	25 ± 4	0.5 ± 0.5	28 ± 11	14 ± 6
40	22 ± 4	0.5 ± 0.5	25 ± 10	14 ± 6
50	19 ± 4	0.5 ± 0.5	25 ± 10	12 ± 6
60	16 ± 4	0	22 ± 10	11 ± 6
70	12 ± 4	0	22 ± 10	9 ± 5
80	10 ± 3	0	17 ± 10	4 ± 5
90	10 ± 3	0	17 ± 10	4 ± 5
100	8 ± 3	0	17 ± 10	4 ± 5
150	3 ± 2	0	7 ± 7	4 ± 5
200	2 ± 2	0	7 ± 7	0
250	0	0	7 ± 7	0

An investigation of the numbers in table II shows that fractions taken for the final distributions are without exception clearly smaller than those taken for the nascent distribution. This consistency is a strong indication for extensive breakup of large clusters.

C. Size distribution of clusters

The cluster size distribution data $(n, Y(n)) \equiv (n, N(n)/N_{\text{ions}})$, where $N(n)$ is the number of clusters containing n atoms and N_{ions} is the number of impinging ions, have been fitted to the inverse power law $Y(n) = Y_1 n^{-\delta}$. Here $Y(n)$ is called the partial yield or alternatively the cluster yield.

During the fitting procedure it became obvious that the fitted exponent δ depends strongly on the lower limit of the data set. This is illustrated in figures 3 and 4, where exponents δ obtained for the data sets $n \geq n_1$ (in-

cluding data points with $Y(n) = 0$) with $n_1 = 1, 2, \dots$, are listed. In order to facilitate comparison between figure 3 and figure 4, the partial yields $Y(n)$ have been normalized to the yield of monomers, $Y(1)$. Note that the various curves have all been plotted for $n \geq 1$ although they are fitted to subsets of this interval.

It should be noted that for the sake of clarity in plotting, the data for intermediate and large clusters have been summed up in order to get rid of points with zero partial yield in figures 3 and 4. Specifically, data points in the interval $n \in [n_a, n_b]$ were replaced by a single point (n', Y') , where $n' = (n_a + n_b)/2$ and $Y' = (Y(n_a) + \dots + Y(n_b))/(n_b - n_a + 1)$. We emphasize that when fitting the data to the inverse power law, we used the original data without any summing up. It was checked that fits to the summed up data gave results for δ reasonably close to the above results.

From the curves in figure 3, it is clear that the inverse power law is a good fit only for the data $n \geq 4$. The fits to the silver data³⁵ behave in a similar manner, this can be concluded from figure 4. The behavior is not as dramatic as for the gold case, but can nonetheless be observed in part (b) of the figure, where the dimer point clearly deviates from the other points.

In table III we present the values of the exponent δ obtained from the best fits of cluster data (usually for $n \geq 4$) to the inverse power law $Y(n) = Y_1 n^{-\delta}$. In order to make our results comparable to studies where all cluster data have been used for the fitting, we also present exponents fitted to all cluster sizes (including monomers). These values are labeled ' $n \geq 1$ '.

We would like to stress that for the results in table III and in figures 3 and 4 only clusters moving away from the surface have been considered. This makes the results directly comparable to those obtainable from experiments.

TABLE III: Representative values for the inverse power law exponent δ for (large) clusters. The label ' $n \geq 1$ ' indicates that all cluster sizes (including monomers) were considered in the fit.

	Ag	Au
	15 keV Xe	20 keV Xe
nascent	2.5 ± 0.1	1.8 ± 0.4
final	3.0 ± 0.4	2.3 ± 0.6
nascent, $n \geq 1$	2.06 ± 0.02	2.84 ± 0.06
final, $n \geq 1$	3.19 ± 0.03	3.51 ± 0.08

D. Temperature of nascent and final clusters

The internal temperature $T(n, t)$ at a time t of a cluster containing n atoms having the masses m_i and the velocities $\mathbf{v}_i(t)$ is obtained from the equipartition theorem:

$$E_{\text{int}}(n, t) = K_{\text{int}}(\{\mathbf{v}_i\}, n) + U(\{\mathbf{r}_i\}, n) + E_a(n)$$

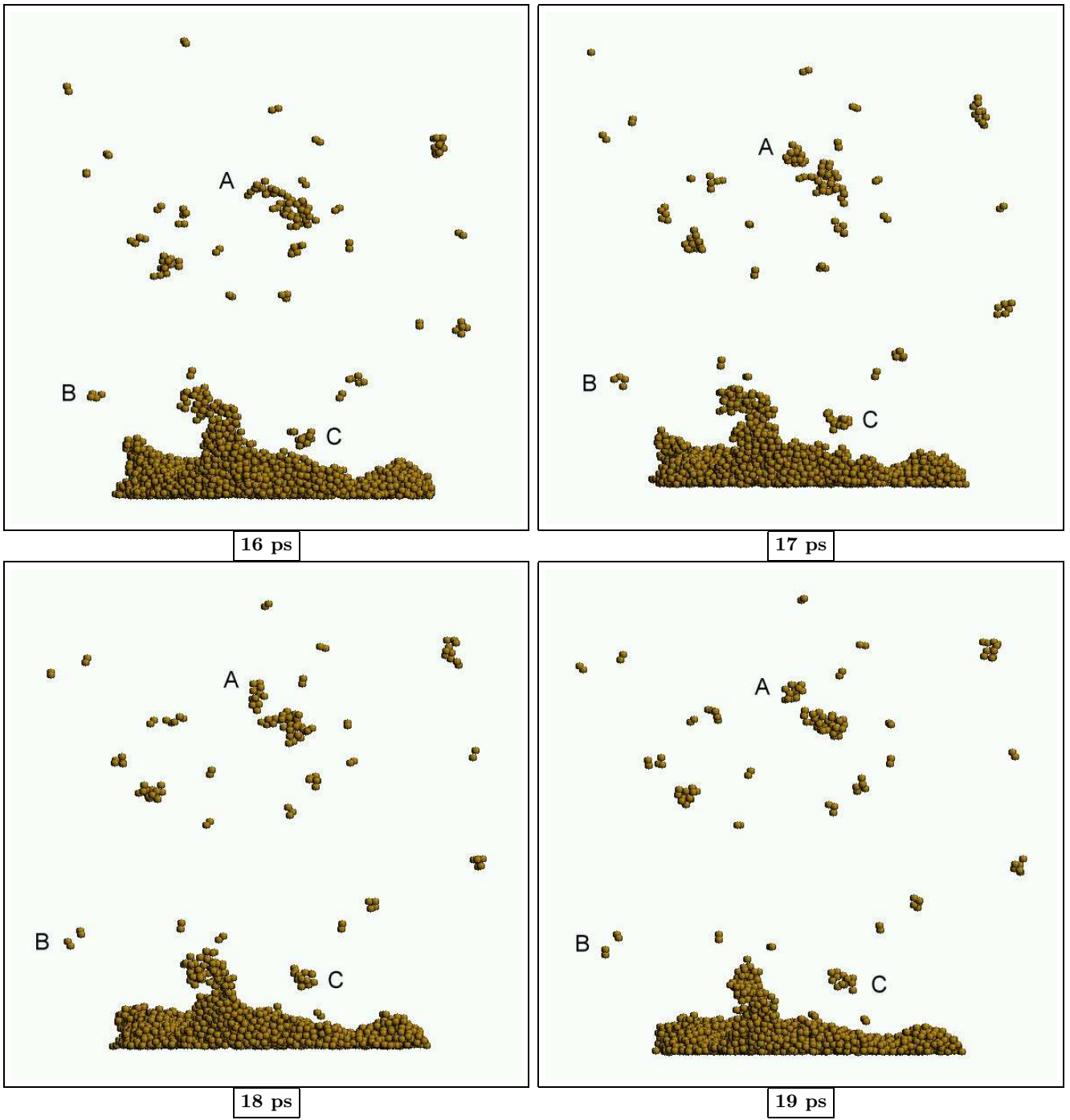
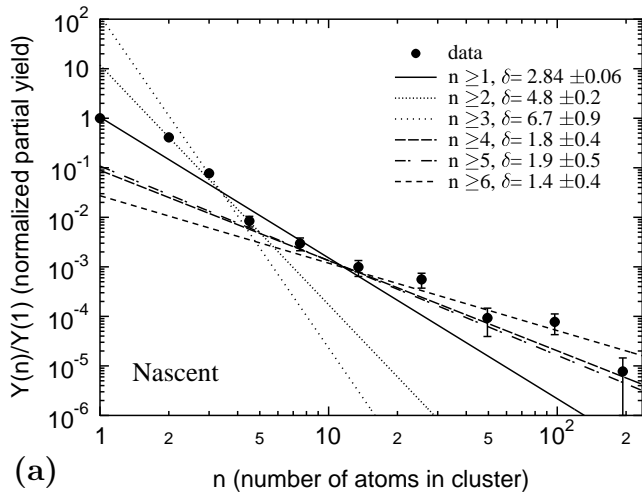


FIG. 2: Snapshots from a simulation of 20 keV Xe incident on Au. Displayed is a part of the sputtered material at times between 16 and 19 ps. The large continuous group in the lower part of the figures is the crater rim that has been formed on the surface by the impinging ion. The labels 'A' and 'B' show clusters that are fragmenting, and 'C' illustrates late sputtering (a cluster separating from the surface after the displacement cascade has ended).

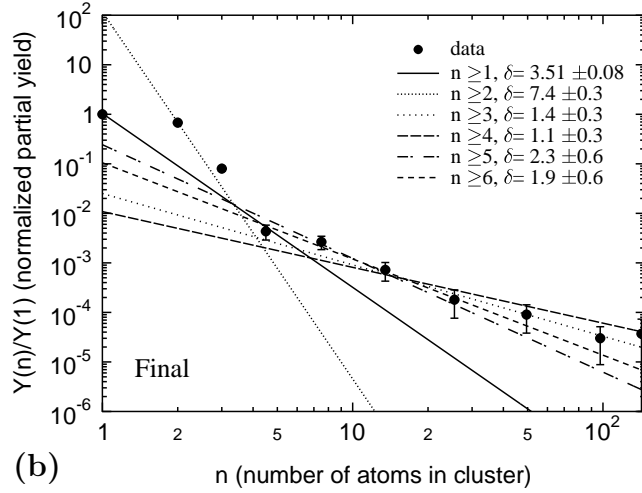
$$\begin{aligned}
 &= \frac{1}{2} \sum_{i=1}^n m_i (\mathbf{v}_i(t) - \mathbf{v}_{\text{CM}}(t))^2 \\
 &\quad + U(\{\mathbf{r}_i\}, n) + E_a(n) \\
 &= 3nk_B T(n, t). \tag{3}
 \end{aligned}$$

Here $E_{\text{int}}(n, t)$ is the internal energy of the cluster, K_{int}

is the internal kinetic energy, U is the potential energy ($U < 0$) and E_a is the atomization energy, *i.e.* minus one times the energy of the ground state of the cluster. If $U = -E_a$, *i.e.* the configuration of the atoms corresponds to the ground state, then the contribution $U + E_a$ is zero, as should be expected. In the equation, $\mathbf{v}_{\text{CM}}(t)$ is



(a) n (number of atoms in cluster)



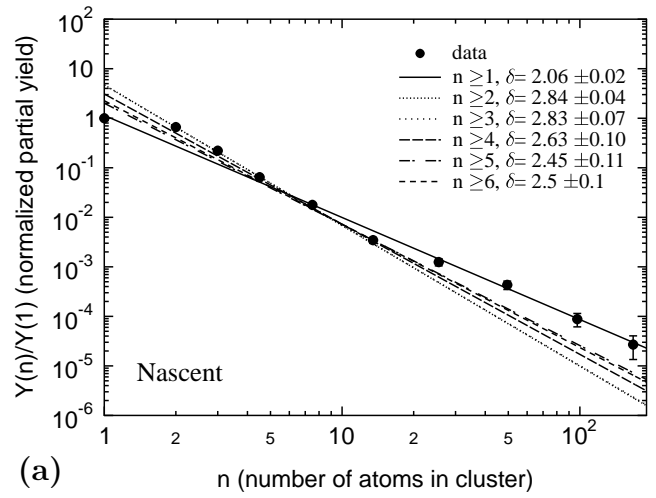
(b) n (number of atoms in cluster)

FIG. 3: Monomer-normalized size distributions of (a) nascent and (b) final clusters for 20 keV Xe on Au fitted to the power law $Y(n) = Y_1 n^{-\delta}$, using the data sets $n \geq n_1$, $n_1 = 1, \dots, 6$. The largest cluster detected contained N atoms. For the nascent clusters $N = 256$, and for the final clusters $N = 154$. The error bars represent one standard deviation. The original data have been summed up in order to remove points with zero yield. Note that the curves have been plotted for $n \geq 1$ although they are fitted to subsets of this interval.

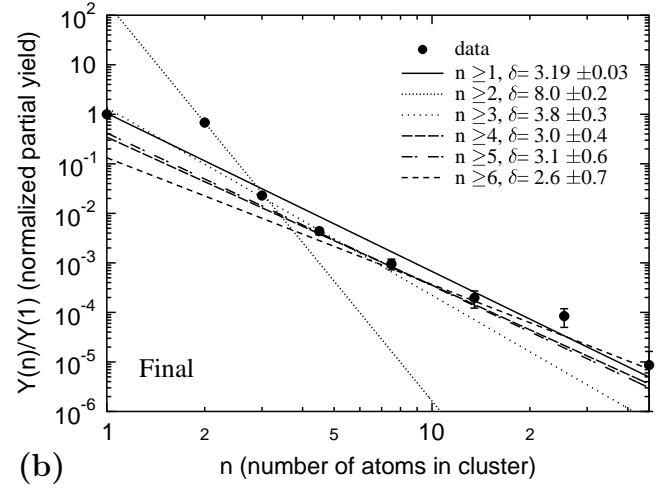
center of mass (CM) velocity for the cluster at time t . A liquid drop expansion was used to fit the atomization energy calculated from simulations of spherical clusters (compare with section IID).

Sometimes the vibrational temperature is calculated instead of the "total" temperature defined in eq. (3), then with $3n$ replaced by $3n - 6$, meaning that three degrees of freedom (DOF) for the motion of the CM and three DOF for the rotation of a nonlinear molecule have been subtracted (ref. 26, p. 361).

The internal energies of nascent and final clusters resulting from the 15 keV Xe on Ag bombardment are



(a) n (number of atoms in cluster)

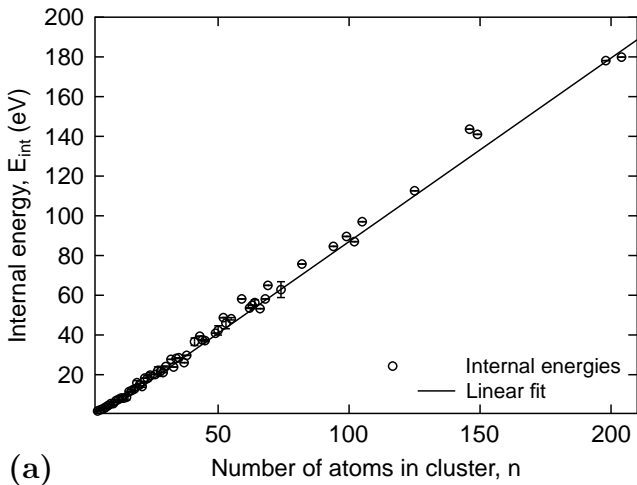


(b) n (number of atoms in cluster)

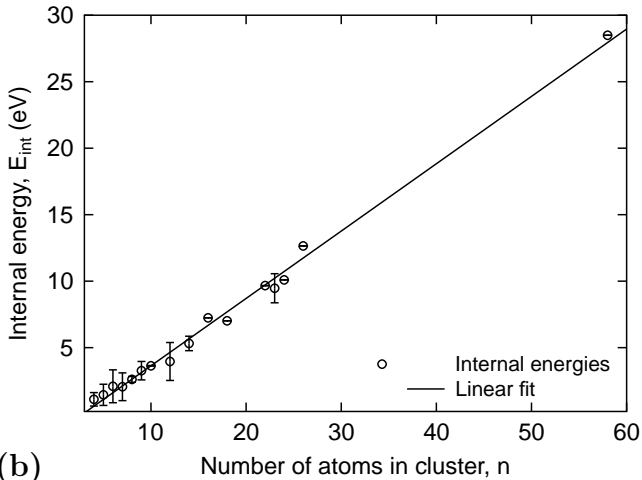
FIG. 4: As for figure 3, but for 15 keV Xe on Ag. For the nascent clusters $N = 204$, and for the final clusters $N = 58$.

displayed in figure 5 (Corresponding temperatures for 20 keV Xe on Au were not calculated and will not be discussed.). Note that the temperatures have been calculated for 'large' clusters only, containing $n \geq 4$ atoms.

Using the fitting function $E(n) = an - b$ we obtain $a = 0.924 \pm 0.002$ eV, $b = 5.38 \pm 0.08$ eV for the nascent clusters and $a = 0.51 \pm 0.02$ eV, $b = 1.4 \pm 0.2$ eV for the final clusters. These fits and the graphs in figure 5 indicate that the temperature of the clusters to a good approximation is independent of the cluster size. We estimate the average cluster temperature by first calculating the average temperatures of individual clusters from eq. (3), and then taking the uncertainty-weighted average³⁶ of these temperatures. Using synthetic uncertainties $0.5T_i$ for temperatures T_i lacking an uncertainty, we obtain the temperatures 3026.20 ± 0.03 K for nascent clusters, and 1406 ± 9 K for final clusters.



(a)



(b)

FIG. 5: Internal energy of (a) nascent and (b) final clusters as a function of cluster size n , with $n \geq 4$. The error is the standard error.

IV. DISCUSSION

A. Total yield

As reported in table I, the total sputtering yield for the MD/MC-CEM potential is 32 ± 7 based on 20 simulations of 20 keV Xe on Au. This can be compared with the EAM value 82 ± 15 . Clearly, the agreement between these two potentials is poor.

From our previous work we know that an accurate melting temperature is an important parameter in simulations of surface-near cascades²⁷. Considering the different melting temperatures for gold mentioned in sec. II, 1635 ± 5 K for MD/MC-CEM, and 1110 ± 20 K for EAM, one can calculate that these values are $122.3 \pm 0.4\%$ (MD/MC-CEM) and $83 \pm 1\%$ (EAM) of the experimental value, 1337 K. Although the difference between these

two values concerning the deviation from 1.000 is not that large, it is noteworthy that the MD/MC-CEM potential presumably makes the substrate less prone to melt locally, thereby somewhat suppressing the thermal spike important in these kinds of cascade simulations.

In general, our results of 129 ± 14 (15 keV Xe on Ag) and 78 ± 13 (20 keV Xe on Au) for the total sputtering yields are quite different from the experimental ones, which are 20 for 15 keV Xe on Ag, and 26 for 20 keV Xe on Au (ref. 28). This discrepancy is possibly best explained by the polycrystalline nature of the experimental samples.

Since the crystal planes and the channels in a polycrystalline sample are randomly oriented, some fraction of all impinging ions are certainly going to be channeled away from the surface. When this happens, the number of thermal spikes created close to the surface is reduced, which in turn decreases the amount of sputtered material. Experimentally it is known that channeling can decrease sputtering yields by a factor of 2 – 4 (ref. 29). Since we used optimal non-channeling directions for the impinging ions in the present study (see sec. II), only the channeling concept itself may suffice to explain the difference between our sputtering yields and the experimental ones, at least for the case of 20 keV Xe on Au.

The discrepancy between experimental sputtering yields and the present results can of course also be due to inaccuracies in the interatomic potential. We will not attempt to review the advantages and disadvantages of the EAM formalism as compared to other models of atomic interaction in metals here. Instead it may suffice to compare theoretical (simulated) and experimental (measured) values for the most relevant and important material parameters.

To simplify matters, one could consider only the following physical quantities to be of significant importance in simulations of surface-near cascades and ejection of atoms and clusters: surface energy, surface binding energy, cohesive energy and melting temperature. If the potential predicts too small values for one or several of these quantities (as compared to experiments) then it seems likely that the formation of a large, hot cascade and subsequent surface rupture and ejection of material would occur 'too easily', resulting in sputtering yields that are too large.

Concerning the surface energy, an average over the (001), (110) and (111) faces of Ag and Au gives 56% and 60%, respectively, of the experimental value (calculated for liquid-metal surfaces¹⁴).

The surface binding energy equals the energy required to remove an atom from the surface of a material. A common approximation³⁰ is to use the heat of sublimation, which equals the heat required for a unit mass of material to change from a solid to a gaseous state. Now, the EAM potentials for Ag and Au are actually fitted to the sublimation energies¹⁴, so simulations and experiments should be in good agreement when it comes to surface binding energies.

The cohesive energy is defined as the minimum total potential energy of an atomic system, divided by the number of atoms. The cohesive energies (which are related to the sublimation energies) are in close agreement with the experimental ones. The ratio of simulated and experimentally measured values is 96.5% for Ag and 99.7% for Au (ref. 19), so no significant inaccuracy should result from this parameter.

The melting temperature is $1150/1235 = 93\%$ (ref. 19) for Ag and 83% for Au, of the experimental value.

From this brief comparison between simulations and experiments it appears that the smallness of the surface energy is the worst deficiency of the potential in the present context. A too low surface energy means that for a given amount of energy and otherwise similar conditions, more surface area can be created in simulations than in experiments. Since the heat spike is directly responsible for some of the ejected material, especially that which comes from loosely bound finger-like features near the surface (see figure 2 and ref. 31), a too low surface energy might well lead to enhanced sputtering. Quantification of this effect would, however, require an extensive, systematic comparison between sputtering yields calculated for potentials with different surface energies, and is beyond the scope of the present study. Hence we cannot at this moment state with certainty whether the reason for the apparent discrepancy in the simulated and experimentally measured sputtering yields is due to the channeling-related uncertainty mentioned above, or inaccuracies in the potential.

B. Fraction of atoms in large clusters

As stated in section IIIB, we find that the breakup of large clusters is significant. In order to further illustrate this, we can for example take the simulation of 20 keV Xe on Au that contained the largest cluster, consisting of 256 atoms. At about 6000 ps this cluster had decayed into a 154-atom cluster, 60% of the original size. For 15 keV Xe on Ag, one run contained a large cluster with 198 atoms at the end of the cascade, as well as four other clusters with 10 or more atoms. At 1000 ns after the cascade had ended, only clusters with 9 atoms or less remained.

The largest nascent clusters that have been observed in other simulation studies contained less than about 40 atoms (0.25 – 5 keV Ar on Ag in ref. 15) and less than about 10 atoms (0.5 – 5 keV Ar on Ag in ref. 16; 2m keV Ag_m ($m = 1, 2, 3$) impacts on Ag in ref. 25). In some experimental studies clusters up to 60 atoms (15 keV Xe on Ag in ref. 5) and up to 200 atoms (15 keV Xe on In in ref. 6) have been observed. Thus, our largest clusters — containing about 250 atoms for the nascent distribution and about 150 atoms for the final distribution — are comparable to those in other simulations and experiments.

C. Size distribution of clusters

1. Silver

The inverse power law exponents for the final size distributions of 15 keV Xe impacts on Ag are 3.0 ± 0.4 when using $n \geq 4$, and 3.19 ± 0.03 when using $n \geq 1$, as indicated in table III. These results are in good agreement with the value 3.3 obtained by Staudt *et al.* in a study of 15 keV Xe impacts on Ag (ref. 5). The authors initially found an exponent of 3.7, but it turned out that this value did not give enough weight to the large clusters. To correct for this, the clusters were accelerated before entering the detector. This correction by post-acceleration is founded on the observation that larger clusters are less easily detected than smaller ones, due to their smaller kinetic energy^{5,6}.

The correction for detection probability of large clusters turned out to have a more dramatic effect when it was applied to indium clusters produced by 15 keV xenon impacts. In this case Staudt *et al.*⁶ obtained an exponent of 3.9, but when taking the said correction into account this value decreased to 2.1. This resulted in two different fitting regimes, namely $n \in [1, 20]$ and $n \in [20, 100]$. The exponent value 3.9 belongs to the former interval, whereas the value 2.1 applies to the latter interval.

The exponents for the nascent size distributions of 15 keV Xe impacts on Ag are 2.5 ± 0.1 when using $n \geq 6$, and 2.06 ± 0.02 when using $n \geq 1$, as indicated in table III. The former value is in reasonable agreement with the results from other simulations, most notably the result $\delta = 2.9$ obtained for 5 keV Ar impacts on Ag (111) surface by Wucher¹⁵ (using the EAM potential) and for 6 keV Ag_3 impacts on Ag (111) by Lindenblatt *et al.*²⁵ (using the MD/MC-CEM potential).

2. Gold

The inverse power law exponents for the final size distributions of 20 keV Xe impacts on Au are 2.3 ± 0.6 when using $n \geq 5$, and 3.51 ± 0.08 when using $n \geq 1$, as indicated in table III. The value for large clusters is in good agreement with that obtained by Rehn *et al.* for 400 – 500 keV Ne, Ar, Kr, Au impacts on Au (ref. 4). In this experiment an exponent of 2.00 ± 0.05 was found. Contrary to the studies referenced above, this study utilized transmission electron microscopy (TEM) to detect the clusters and establish their size distribution, thereby circumventing the possible complications inherent in the single-photon ionization technique^{3,7} (see section IID).

The exponents for the nascent size distributions of 20 keV Xe impacts on Au are 1.8 ± 0.4 when using $n \geq 4$, and 2.84 ± 0.06 when using $n \geq 1$, as indicated in table III. The value for large clusters is in good agreement with the results obtained by Kissel and Urbassek³² in a molecular dynamics study of 100 keV Au incident on spherical Au clusters having a radius of about 40 Å. The authors found

a power law exponent of 2.3 at 20 ps after ion impact. The exponent value showed a slight increase amounting to 5% when the time was extended to 30 – 100 ps, which gives a rough value of $\delta = 2.4$.

3. Fitting range

We would like to stress the importance of the lower limit of cluster sizes when fitting the size distribution to the inverse power law. It was pointed out in section III C that the fitting range can have quite a significant effect on the value of the exponent. This sensitivity seems to be due to the fact that the dimer yield tends to be ‘too large’ as compared to the monomer and trimer yields, as observed in our simulations and in experiments⁵ carried out for 15 keV Xe impacts on Ag. However, the dimer contribution to the size distribution of final clusters does not show any pronounced deviation in the MD/MC-CEM simulation studies by Wucher *et al.*¹⁶ of Ar impacts on Ag (111) and Lindenblatt *et al.*²⁵ of Ag_m ($m = 1, 2, 3$) impacts on Ag (111). Also, the experimental results² quoted in ref. 16 do actually suffer from a similar ‘over-production’ of dimers: the dimer yield deviates clearly from that of monomers and trimers.

These observations raise the question if it is correct to consider the cluster size distribution being well approximated by a power law. After all, if the data for small clusters (say, those containing less than four atoms) are consistently in conflict with the power law model based on data for large clusters, then the true model expression cannot be a power law.

In several studies^{4,6,15} the shock-wave model for cluster sputtering developed by Bitensky and Parilis⁸ is preferred over the thermodynamical model of Urbassek⁹ when it comes to explaining the observed dependence of the partial yield $Y(n)$ on the cluster size n . The former model predicts an asymptotical power law dependence $Y(n) = Y_1 n^{-\delta}$ with $\delta = 5/3 \approx 1.7$ or $\delta = 7/3 \approx 2.3$, *i.e.* $\delta \sim 2$. A similar asymptotical behavior is observed in our results. Therefore, instead of inventing a new model we consider our results being well modeled by an inverse power law, that holds in an asymptotical sense.

4. Nascent versus final exponents

Since in most simulation studies and experiments referenced here the largest cluster contains of the order of 100 atoms *and* the fitting of data to an inverse power law usually makes use of all clusters — even the sometimes dominating monomer and dimer contributions — it seems appropriate to ask whether the result for the power law exponent obtained from these size distributions really can be compared to the analytical prediction.

A study which is not limited in this respect is that by Rehn *et al.*⁴, where clusters with more than 500 atoms were observed. As mentioned previously, an exponent of

$\delta = 2$ was obtained in this case, and thus seems to provide compelling evidence for the Bitensky-Parilis shock wave model. However, this result is for the *final* size distribution, established when the clusters had traveled about 30 μm from the irradiated target. The Bitensky-Parilis model applies only to the *nascent* clusters, since the model does not describe the fragmentation of clusters that takes place when they move from the irradiated surface to the detector.

From table III it seems that the (representative) values of the exponents δ_1 and δ_2 for the size distribution of nascent and final clusters, respectively, are relatively close to each other. A calculation shows that the ratio $r \equiv \delta_2/\delta_1$ is 1.2 ± 0.2 for 15 keV Xe on Ag, and 1.3 ± 0.4 for 20 keV Xe on Au. Similar findings of 1.3 and 1.4 when using the EAM potential, and 1.2 when using the MD/MC-CEM potential (error limits unknown) have been obtained in simulation studies^{15,16}.

Assuming that these ratios have a real physical basis and are transferable to other ion and substrate types, one can estimate that the nascent exponent in the experiment by Rehn *et al.*⁴ should be $\delta_1 = \delta_2/r = 2.0/r = 1.5 - 1.7$, taking r to be between 1.2 and 1.3. The value of 1.7 actually coincides with the lower value $\delta_1 = 5/3 \approx 1.7$ mentioned by Bitensky and Parilis⁸. Similarly, one obtains $\delta_1 = \delta_2/r = 2.1/r = 1.6 - 1.8$ for the experimental result $\delta_2 = 2.1$ obtained by Staudt and Wucher⁶ when bombarding In with 15 keV Xe, for clusters in the range $n \in [20, 100]$.

From the present results it appears that although the fragmentation of nascent clusters causes the inverse power law exponent to grow, this change does not need to be very dramatic. Considering the values $r = 1.2 \pm 0.2$ for 15 keV Xe on Ag and $r = 1.3 \pm 0.4$ for 20 keV Xe on Au found in the present study, the growth $\delta_1 \Rightarrow \delta_2 \equiv r\delta_1$ may be limited by a factor of $1.0 < r \leq 1.7$, considering the uncertainties.

D. Temperature of nascent and final clusters

For 15 keV Xe on Ag it was observed that the temperatures of nascent and final clusters were more or less independent of cluster size. Average temperatures of 3026.20 ± 0.03 K and 1406 ± 9 K were estimated for nascent and final clusters, respectively. A fit of the internal energies to the expression $E_{\text{int}}(n) = an - b$ gave $a = 0.924 \pm 0.002$ eV, $b = 5.38 \pm 0.08$ eV and $a = 0.51 \pm 0.02$ eV, $b = 1.4 \pm 0.2$ eV for nascent and final silver clusters, respectively.

Similar results of approximately size-independent cluster temperatures have been found in other studies^{15,16,25,33} (simulations and experiments), but for cluster sizes $n \lesssim 10$. The present results extends the size-independence of cluster temperatures to clusters of sizes $n \simeq 200$ for nascent clusters and $n \simeq 60$ for final clusters.

In other simulation studies of the bombardment of Ag

surfaces different parameter values for the size dependence of the internal energy $E_{\text{int}}(n) = an - b$ of clusters containing n atoms have been found. Wucher¹⁵ have investigated 0.25–5 keV Ar impacts on Ag (111) using the EAM potential, and obtained $E_{\text{int}}(n) = 1.54n - 1.65$ eV, $n \leq 13$, for nascent clusters (supposedly for 5 keV ions). In a later study of 0.5–5 keV Ar impacts on Ag (111) using the MD/MC-CEM potential, Wucher and Garrison¹⁶ found that $E_{\text{int}}(n) = 1.40n - 1.86$ eV, $n \leq 10$ (mostly for 5 keV ions). In a study of $2m$ keV Ag_m (with $m = 1, 2, 3$) impacts on Ag (111) using the MD/MC-CEM potential, Lindenblatt *et al.*²⁵ obtained approximately $E_{\text{int}}(n) = 1.57n - 2.54$ eV ($n \leq 7$) for clusters produced by 2 keV Ag ions, $E_{\text{int}}(n) = 1.25n - 1.80$ eV ($n \leq 10$) for clusters produced by 4 keV Ag_2 ions, and $E_{\text{int}}(n) = 1.10n - 1.46$ eV ($n \leq 10$) for clusters produced by 6 keV Ag_3 ions.

This review of earlier results indicates that the prefactor a in the equation $E_{\text{int}}(n) = an - b$ is reduced when the kinetic energy of the projectile is increased. In summary, our value $a = 0.924$ for 15 keV ions is in line with the values $a = 1.10 - 1.57$ obtained for lower energy ions (2–6 keV).

V. CONCLUSIONS

We have obtained the size distribution of nascent and final clusters from sputtering simulations of 15 keV Xe

on Ag and 20 keV Xe on Au. Fits to an inverse power law resulted in exponents that are in good agreement with those obtained from other studies. We have showed that the choice of fitting range can have a large impact on the exponent, since especially the dimer and trimer partial yields can deviate from a simple power law. For the particular cases of heavy ion irradiation of silver and gold studied here, the results show that clusters are subject to massive breakups, which reduce the size of the largest cluster by a factor of 2–4 when comparing nascent and final clusters. Nevertheless, the exponent δ in the size distribution $Y(n) = Y_1 n^{-\delta}$ of sputtered clusters is nearly the same for nascent and final clusters: considering the uncertainties, the increase is limited to a factor of 1.0–1.7.

Acknowledgments

We would like to thank Dr. Emppu Salonen for useful and critical comments on the manuscript, and Prof. B.J. Garrison for making the MD/MC-CEM potential parametrization for gold available to us. We also thank Prof. A. Wucher and Dr. L. Rehn for useful discussions. The research was supported by the Academy of Finland under project No. 48751 and by the University of Helsinki under the NAPROMA project. Grants of computer time from the Center for Scientific Computing in Espoo, Finland are gratefully acknowledged.

* Electronic address: krister.henriksson@helsinki.fi

¹ W. Hofer, in *Sputtering by Particle Bombardment III*, edited by R. Behrisch and K. Wittmaack (Springer, Berlin, Germany, 1991), chap. 2, pp. 15–256.

² M. Wahl and A. Wucher, Nucl. Instr. Meth. Phys. Res. B **94**, 36 (1994).

³ A. Wucher, M. Wahl, and H. Oeschner, Nucl. Instr. Meth. Phys. Res. B **82**, 337 (1993).

⁴ L. E. Rehn, R. C. Birtcher, S. E. Donnelly, P. M. Baldo, and L. Funk, Phys. Rev. Lett. **87**, 207601 (2001).

⁵ C. Staudt, R. Heinrich, and A. Wucher, Nucl. Instr. Meth. Phys. Res. B **164-165**, 677 (2000).

⁶ C. Staudt and A. Wucher, Phys. Rev. B **66**, 075419 (2002).

⁷ A. Wucher and M. Wahl, Nucl. Instr. Meth. Phys. Res. B **115**, 581 (1996).

⁸ I. S. Bitensky and E. S. Parilis, Nucl. Instr. Meth. Phys. Res. B **21**, 26 (1987), and references therein.

⁹ H. M. Urbassek, Nucl. Instr. Meth. Phys. Res. B **31**, 541 (1988).

¹⁰ K. Nordlund, M. Ghaly, R. S. Averback, M. Caturla, T. D. de la Rubia, and J. Tarus, Phys. Rev. B **57**, 7556 (1998).

¹¹ E. M. Bringa, K. Nordlund, and J. Keinonen, Phys. Rev. B **64**, 235426 (2001).

¹² K. Nordlund, Comput. Mater. Sci. **3**, 448 (1995).

¹³ H. J. C. Berendsen, J. P. M. Postma, W. F. van Gunsteren, A. D. Nola, and J. R. Haak, J. Chem. Phys. **81**, 3684 (1984).

¹⁴ S. M. Foiles, M. I. Baskes, and M. S. Daw, Phys. Rev. B

33, 7983 (1986).

¹⁵ A. Wucher, Nucl. Instr. Meth. Phys. Res. B **83**, 79 (1993).

¹⁶ A. Wucher and B. Garrison, J. Chem. Phys. **105**, 5999 (1996).

¹⁷ C. Kelchner, D. Halstead, L. Perkins, N. Wallace, and A. DePristo, Surf. Sci. **310**, 425 (1994), and references therein.

¹⁸ J. F. Ziegler, J. P. Biersack, and U. Littmark, *The stopping and range of ions in matter* (Pergamon, New York, USA, 1985).

¹⁹ D. R. Lide, *CRC Handbook of Chemistry and Physics* (CRC Press LLC, Boca Raton, FL, USA, 2001), 82nd ed.

²⁰ L. J. Lewis, P. Jensen, and J.-L. Barrat, Phys. Rev. B **56**, 2248 (1997).

²¹ S. J. Zhao, S. Q. Wang, Z. Q. Yang, and H. Q. Ye, J. Phys.: Condens. Matter **13**, 8061 (2001).

²² K. Elihn, L. Landström, and P. Heszler, Appl. Surf. Sci. **186**, 573 (2002).

²³ P. Heszler, L. Landström, M. Lindstam, and J. O. Carlsson, J. Appl. Phys. **89**, 3967 (2001).

²⁴ A. Wucher and B. J. Garrison, Phys. Rev. B **46**, 4855 (1992), and references therein.

²⁵ M. Lindenblatt, R. Heinrich, A. Wucher, and B. Garrison, J. Chem. Phys. **115**, 8643 (2001).

²⁶ F. Mandl, *Statistical Physics*, Manchester Physics Series (Wiley, Chichester, UK, 1988), 2nd ed.

²⁷ K. Nordlund, K. O. E. Henriksson, and J. Keinonen, Appl. Phys. Lett. **79**, 3624 (2001).

- ²⁸ H. Andersen and H. Bay, in *Sputtering by Particle Bombardment I*, edited by R. Behrisch (Springer, Berlin, Germany, 1981), vol. 47 of *Topics in Applied Physics*, chap. 4.
- ²⁹ H. E. Roosendaal, in *Sputtering by Particle Bombardment I*, edited by R. Behrisch (Springer, Berlin, Germany, 1981), vol. 47 of *Topics in Applied Physics*, chap. 5, pp. 219–256.
- ³⁰ J. F. Ziegler, *SRIM Instruction Manual* (2004), <http://www.srim.org>.
- ³¹ K. Nordlund, J. Tarus, J. Keinonen, S. E. Donnelly, and R. C. Birtcher, *Nucl. Instr. Meth. Phys. Res. B* **206**, 189 (2003).
- ³² R. Kissel and H. Urbassek, *Nucl. Instr. Meth. Phys. Res. B* **180**, 293 (2001).
- ³³ A. Wucher, N. K. Dzhemilev, I. V. Veryovkin, and S. V. Verkhoturov, *Nucl. Instr. Meth. Phys. Res. B* **149**, 285 (1999).
- ³⁴ P. R. Bevington and D. K. Robinson, *Data reduction and error analysis for the physical sciences* (McGraw-Hill, 2003), 3rd ed.
- ³⁵ It should be noted that when taking the natural logarithm

of the data values and fitting to a correspondingly modified function ("making a log-fit") the resulting δ values are somewhat different (generally smaller). However, the dependence on the fitting interval $n \geq n_1$, $n_1 = 1, \dots, 6$, is similar. Also, it is important to realize that in the present case a constant must be added to all data points in order to remove points with zero partial yield and make a log-fit possible. In the fitting procedure it turned out that the value of this constant influences the fit. For example, fits to all partial yield points for final silver clusters using additive constants of 1 and 10, respectively, produces δ values that differ by about 30%. Due to this complication, the results presented in the main text are those of a direct fitting without using logarithms.

³⁶ The average is defined as $\langle T \rangle = (\sum_i T_i / \sigma_i^2) / (\sum_i 1 / \sigma_i^2)$ and its uncertainty (standard deviation) is $\sigma_T = \sqrt{(\sum_i 1 / \sigma_i^2)^{-1}}$. See ref. 34.